International Journal of Offshore and Polar Engineering
Vol. 11, No. 3, September 2001 (ISSN 1053-5381)

Hydrodynamics in the Swash Zone

Marco Petti*
Dipartimento di Georisorse e Territorio, University of Udine, Udine, Italy

Sandro Longo
Dipartimento di Ingegneria Civile, University of Parma, Parma, Italy

ABSTRACT

This paper describes a study of the hydrodynamics in the swash zone using an impermeable concrete beach in a laboratory flume. Analysis was made of the measurements achieved using level wave gauges and a laser Doppler velocimeter. From these measurements we could derive the mean motion and turbulence characteristics along the main flow direction in 3 vertical sections of the swash zone. Fluid velocity seems almost uniform along the vertical, especially during the up-rush; the behaviour of turbulence dynamics is a mixture of free turbulence generated during wave breaking and convected by the mean motion, and wall turbulence. This work covers analysis in the time and frequency domain, and discusses the turbulent properties of the flow field derived from our measurements.

INTRODUCTION

Coastal region management is becoming increasingly important and requires a detailed knowledge of the numerous phenomena that occur near the coast. There are several problems to solve, connected with sediment transport, pollutant dynamics, currents and waves near harbours and beaches; thus many numerical models have been developed and successfully applied. The first models, based on a linear approach, have led to a better understanding of the dynamics of sea waves, solving wave propagation and wave-structure interaction in deep and shallow water. Their conceptual and computational simplicity leads to some engineering applications and indeed these models are successfully used, even though it is well known that there is a fair amount of nonlinear behaviour. For the most complex cases, the results of linear models are used as a first approximation to address more detailed approaches.

The dream of numerical researchers is to integrate the full Navier-Stokes equations, but this is not feasible, due to the computational limitations at a high Reynolds number even in limited integration domains. A relatively simpler approach is the integration of the shallow-water or Boussinesq equation, a depth-integrated version of the Euler equations for potential flow (Mei, 1989; Abbott, 1978, 1979). In 1989, Deigaard and Fredøse introduced the roller concept, modelled as an hydraulic jump, and suggested possible modifications of the Boussinesq equation to take into account the dissipation occurring in the shear layer beneath the surface roller. A lot of researchers proposed modified Boussinesq equations, adding a dissipation term to the depth-integrated momentum equation. Karambas and Koutitas (1992) modelled turbulence using the eddy viscosity concept; Schäffer et al. (1993) used the roller concept proposed by Deigaard and Fredsøe; Drago and Iovenitti (1995) used both concepts, evaluating the eddy viscosity by a k-l equation model. Even though a calibration of the parameters associated with these models was required, all authors found their results tied in with laboratory data in terms of wave height evolution in the surf-zone; very good results were obtained for spilling breaking rather than for plunging, but this was expected from the roller assumption. Knowledge of the velocity field in the surf and swash zone is very important in understanding the dynamics that govern sediment transport, one of the main problems in coastal regions. On observing that the accuracy of the velocity field obtained from the above-mentioned models had not been established, Lin and Liu (1998) proposed a k-ε model based on the nonlinear Reynolds stress model with a new evaluation of the empirical coefficients. Good results were obtained in terms of free-surface profiles, mean velocities and turbulent kinetic energy for shoaling and breaking cnoidal waves.

At present, the researchers' opinion is that depth-integrated models are unable to adequately predict dynamics in the inner surf zone and swash zone, where the turbulence generated by breaking and at the bottom spreads in the fluid domain. Models based on 2-D Reynolds equations in the main flow direction and in the vertical, with closure equations, appear to be more promising. Of course, such an approach requires a good understanding of the turbulence characteristics involved to make an appropriate closure. These can be understood mainly via laboratory experiments.

Many researchers have studied the turbulence dynamics in the surf zone, as seen by the works of Stive (1980), Nadaoka et al. (1989), Flick and George (1990); more recent work has been done by Ting and Kirby (1994,1995,1996), Pedersen et al. (1998), Rodriguez et al. (1999). However, most have focused mainly on the outer or inner surf zone instead of the swash zone, often considering the swash zone as an inner part of the surf zone. In reality, the swash zone is the region where the up-rush/backwash cycle occurs on the beach face, thus the bottom in this region is periodically wet and dry; in the most landward sections, the still water level is simply not defined. Thus some of the classical scales used in surf zone analyses cannot be used here. First of all, then, new scales have to be defined to describe the turbulence dynamics in the swash zone.

---

* ISOPE Member.
Received September 25, 2000; revised manuscript received by the editors April 25, 2001. The original version (prior to the final revised manuscript) was presented at the Tenth International Offshore and Polar Engineering Conference (ISOPE-2000), Seattle, USA, May 28–June 2, 2000.
KEY WORDS: Turbulence, swash zone, wave breaking.

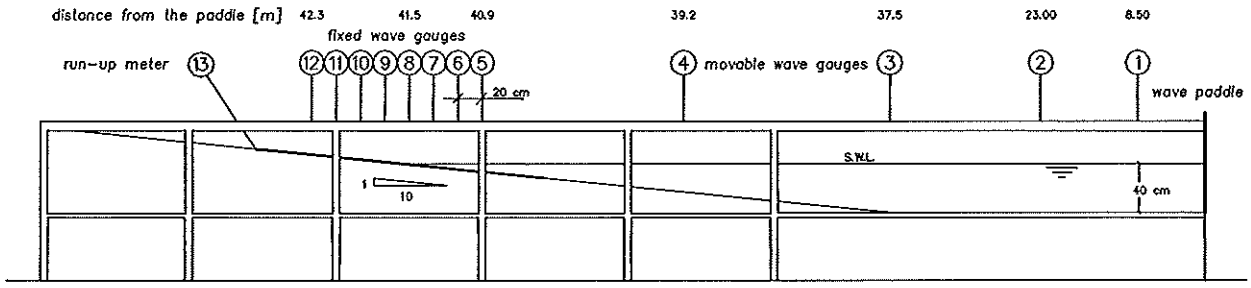

Fig. 1 Experimental setup and location of wave gauges. Location of each wave gauge given as 'sec.' in following figures and text below.

The aim of this note is to describe turbulence characteristics in the swash zone using data from flume experiments. The tests refer to regular waves over an impermeable and essentially smooth concrete beach. The measurements were carried out using level gauges and a laser Doppler velocimeter (LDV); detailed analyses were carried out to derive the mean motion and turbulence in 3 vertical sections of the swash zone, equally spaced in the main flow direction.

EXPERIMENTAL SETUP

The experiments were conducted in a wave flume (Fig. 1) 48 m long, 0.8 m wide, and 0.8 m high. At one end of the flume a wave maker was installed. A paddle moved by an electronic-controlled hydraulic system forms this. The displacement of the paddle is controlled by a hydraulic servo-valve, in turn moved by a computer system, through a low-voltage electrical signal; a feedback checks the target paddle displacement.

The computer system consists of a personal computer equipped with an Intel 80586 processor, two boards A/D and D/A 12 bits converters, and analogue low-pass filters. High-level software (Petti, 1988) programmes the run of the waves in the flume and, in real time, to show, collect and store the signals coming from 32 acquisition channels connected to as many gauges.

A concrete-bottom 1:10 sloping beach was built up starting 37.5 m from the paddle; its surface was finished to reduce roughness. Three specimens were collected from that part of the beach out of the maximum water level, assuming that the wave action is not strong enough to smooth the surface. The geometric scale of roughness was evaluated through a detailed analysis of the specimens using a Laser interferometric pickup transverse unit (RTH Form Talysurf-120L), according to ISO 4287. The average height value of the crests is around 30 mm without evident differences among the specimens; the bottom surface is quite regular, without apparent 3-D effects induced on the wave field.

A series of 12 resistive wave gauges were used for water level measurements: 4 movable, at different positions along the flume and 8 fixed, located in the surf and swash zone (Fig. 1).

Of the 4 movable gauges, 3 (1-3) were placed on the plane bottom part of the flume, at distances from the paddle of 8.5, 23 and 37.5 m; their output was used to check the generated waveforms. The fourth wave gauge (4) was positioned 39.2 m from the wave paddle. Eight fixed gauges (5-12) were placed at intervals of 20 cm (the best compromise to avoid reciprocal interference and to cover the measured zone with an adequate resolution) across the swash zone (Fig. 1). Finally, a runup meter (gauge 13) was placed parallel to the bottom in the swash zone, to measure the bore front position. It was insulated from the concrete surface to prevent short-circuiting the resistance and 5 mm away to avoid meniscus and consequent output distortion.

Particular attention was given to the calibration of the gauges in the swash zone, which is characterised by an up-rush/backwash cycle with the gauges becoming wet only for a fraction of the wave period. During backwash, the gauges did not have a linear characteristic around the zero water level; moreover, there was a transient error in the output which reached the correspondent zero level voltage output only after a time interval. This was due to the local conditions at the base of the gauge (residual water around the screws, distortion induced by the concrete bottom). These signals were corrected by detecting the output discontinuity that marks the water front crossing during backwash.

Three regular periodic waves were generated in the flume. Each test was performed strictly maintaining the still water level in the flume as equal to 40 cm, waiting enough time between 2 successive tests in order to get actual still-water conditions, and checking gauge measurements through the acquisition system for the entire length of each test. The whole set of regular wave tests performed is summarised in Table 1, subscript 1 refers to data collected at gauge 1, subscript 0 refers to data estimated in deep water through the linear wave theory; K_r represents the estimated reflection coefficient. For all tests the breaking point, defined as the point at which the crest begins to break, occurred at section 5.

Instantaneous velocities in the swash zone were measured by an LDV system in forward scatter, at several equally spaced points with a 1-mm step, starting 0.5 mm from the bottom, along the verticals of 3 different sections. The 3 sections were at the still water level intersection with the slope (section 8), +20 cm shoreward (section 9), and the last at –20 cm seaward (section 7). The position of the upper section was lowered to +5 cm for test No. 1, rather than x = +20 cm, because stream thickness was not significant in section 9. Many runs for each regular wave were necessary to cover the whole vertical measure for each section, thus a repetitiveness analysis was carried out. This was done successfully by checking the wave height and wave period collected by gauges 1-3 for the whole set of tests.

The acquisition rate was 100 Hz for all the signals collected. Using data collected with gauge 1, taking into account the shoaling effect, surf similarity parameters ξ_b was estimated for each wave train by the relation (Gourlay, 1992):

Test	H_0 (cm)	H_1 (cm)	T (s)	H_0/H_1	ξ_b	breaking type	K_r
No. 1	3.6	3.5	2.0	0.006	0.93	*Plunging*	0.16
No. 2	3.3	3.5	2.5	0.003	1.12	*Plunging*	0.27
No. 3	3.3	3.8	3.0	0.002	1.28	*Collapsing*	0.34

Table 1 Experimental wave conditions

$$\xi_b = \frac{1.45 \cdot \tan(\vartheta)}{(H_0 / L_0)^{0.36}} \tag{1}$$

The results are reported in Table 1; the last column shows the reflection coefficients.

DATA ANALYSES

Analysis of water levels, velocity and turbulence was carried out on the data collected after each test. All data were analysed using the ensemble average (phase average) or a modified version, the conditional sampling ensemble average, and the usual time average. These operators, applied to a generic sampled physical function G, are:

$$\tilde{G}(t) = \frac{1}{N}\sum_{k=0}^{N-1} G(t + kT) \tag{2}$$

$$\text{and} \quad \langle G \rangle = \frac{1}{T}\int_0^T G(t)\, dt \tag{3}$$

where t is the time, ranging between 0 and the wave period T, and N is the number of wave periods sampled. The conditional sampling average is:

$$\tilde{G}(t) = \frac{1}{N}\sum_{k=0}^{N-1} G(t + t_k) \tag{4}$$

where t_k is the time of a trigger event. This last average has been widely used in analysing the present data; the triggering time t_k has been chosen in correspondence with the local minimum water level. Due to small fluctuations, $(t_k - t_{k-1})$ is not exactly equal to the wave period T.

The mean water levels $\tilde{\eta}(t)$ and $\langle\tilde{\eta}\rangle$ were estimated using a conditional average, for each test at each wave gauge to obtain the variations of the free surface and the setup profile (not presented). Similarly, the phase velocity profiles $\tilde{u}(t)$ were calculated at each level from the bottom in sections 7, 8 and 9. Turbulent oscillations $u'(t)$ along the main flow direction may be obtained by subtracting the phase-averaged value $\tilde{u}(t)$ from the instantaneous velocity $u(t)$:

$$u'(t) = u(t) - \tilde{u}(t) \tag{5}$$

Spurious phenomena like the seiches, triggered in the flume by re-reflected wave components, complicate the problem of turbulence estimates. In fact, applying Eq. 5, the organised velocity oscillations $\tilde{u}(t)$ bounded to the seiches remain trapped into the turbulent component $u'(t)$ and the result is that we find the sum $u'(t) + \tilde{u}(t)$ instead of $u'(t)$. Unfortunately a linear low pass filter cannot be used to separate velocity components $\tilde{u}(t)$ and $u'(t)$, because real turbulence may be eliminated. Assuming that the time scale of the turbulence is less or equal to wave period T and that $\tilde{u}(t)$ is a constant rate of the total measured long component $\tilde{u}_m(t)$, on the base of the autocorrelation functions it is possible to estimate the pure component $\tilde{u}(t)$ (Petti, 2001).

The phase-averaged value $\widetilde{u'^2}(z,t)$ represents an estimator of the time-varying turbulent energy at different height levels over the bed.

The autocorrelation $\tilde{Q}(z,\tau)$ and the energy spectral density of the fluctuating velocity $u'(t)$ were evaluated for each record as:

$$\tilde{Q}(z,\tau) = \overline{\langle u'(z,t)\, u'(z,t+\tau)\rangle}, \tag{6}$$

$$\text{and} \quad \tilde{S}(z,f) = \frac{1}{T}\overline{\left|\int_0^T u'(z,t) e^{-i2\pi ft} dt\right|^2} \tag{7}$$

The normalised auto correlation is obtained as:

$$\tilde{R}(z,\tau) = \tilde{Q}(z,\tau) / \overline{\langle u'^2 \rangle} \tag{8}$$

The Eulerian integral time scale T_E was calculated as the area under the normalised autocorrelation:

$$T_E(z) = \int_0^{\tau^*} \tilde{R}(z,\tau)\, d\tau \tag{9}$$

The correspondent spatial scale can be obtained using the frozen turbulence hypothesis (Reynolds, 1974). Taylor's hypothesis represents a zero-order Lagrangian approximation: The fluid particle displacement is related only to the pure translation of the vortex within which it is trapped, disregarding the effects of rotation of the vortices and of acceleration. This hypothesis is valid if the ratio between the fluctuating velocity and the mean velocity is less than ~ 0.1; for all tests it was observed that the ratio of a turbulence estimator $\langle(u'^2(t))^{1/2}\rangle$ and the amplitude of the periodic velocity components $\tilde{u}$ are very close to 0.1. Consequently the diffusion integral length scale Λ is computed as:

$$\Lambda = < \sqrt{\tilde{u}^2} > T_E \tag{10}$$

Note that near the free surface, the fluctuating velocity can be much higher than 10% of the mean velocity, especially during uprush, and Taylor's hypothesis cannot be applied. Unfortunately our measurements do not reach the free surface and are limited to a region where Eq. 10 can be applied with confidence.

Finally, an estimation of the coefficient of eddy diffusion ν_T is given as:

$$\nu_T = < \sqrt{\overline{u'^2}} > \Lambda \tag{11}$$

All analyses have been performed using 170 waves, after checking the steadiness of some statistical parameters: for the mean velocity $\tilde{u}(t)$ and the turbulent oscillations $\langle(u'^2(t))^{1/2}\rangle$ it was found that for a number of waves $N > 80$ deviations from the estimated values are within ±2.5%. As a stationary criterion, we also used a check based on the autocorrelation function $Q(z,\tau)$ estimated for each period. Only the time intervals satisfying the condition:

$$\left|Q(z,\tau) - \tilde{Q}(z,\tau)\right| \le 3\sigma_Q(z,\tau) \tag{12}$$

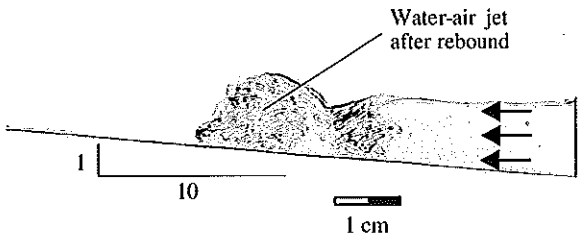

Fig. 2 Flow field geometry immediately after breaking. Dark region is full of air bubbles.

were included, $\sigma_Q(z,\tau)$ being the standard deviation of $Q(z,\tau)$ from $\tilde{Q}(z,\tau)$.

RESULTS AND DISCUSSION

The flow field in the measurement sections looks quite complicated, as can be observed in Fig. 2, obtained by using a video frame. A roller develops and rebounds on the bottom after breaking; a lot of air bubbles are entrained near the free surface and then convected. There are 2 distinct phases of motion, the up-rush and the backwash. The general impression is that in the swash zone, turbulence behaves in the same way as free turbulence (generated during wave breaking and convected by mean motion) during up-rush, and as wall turbulence during backwash. Measurements are quite difficult to make, especially near the free surface, where breaking starts and occurs most of the time, because bubbles and air-entrapment prevent LDV locking. Thus there is a lack of velocity data near the free surface, especially during up-rush.

Fig. 3 shows the phase-averaged free-surface levels for the test with a T = 3.0 s wave period in sec. 7, 8 and 9. The vertical z axis originates at the bottom and is upward; the phase refers to the minimum water level in sec. 8. The breaking point, which occurs in sec. 5, i.e. 60 cm seaward, generates high-frequency free harmonic components that move both landward and seaward, represented by the spikes.

Fig. 4 show the phase-averaged velocity distribution obtained in sec. 7, 8 and 9 for a T = 3.0-s wave; positive values mean a landward direction. The vertical scale is nondimensional with respect to the maximum local water level δ with respect to the bottom, rather than the still water depth or the usual mean water depth. This choice was made because the mean water depth in the swash zone is usually very small, and its influence on the phenomena appears to be very limited. Fig. 4a illustrates the presence of an undertow velocity directed seaward. Phase velocities are quite constant along the vertical during up-rush, while during backwash the bottom seems to have a small amount of influence; this influence is quite evident in sec. 8 (Fig. 4b).

Similar behaviour can be easily seen by analysing horizontal turbulent energy during the up-rush and backwash phases (Figs. 5 and 6). During up-rush, strong turbulence is generated by the breaking in the upper layers near the free surface (Fig. 5a: phase 60°), with limited turbulence near the bottom. In sec. 8 and 9 (Figs. 5b and c), it is evident how the turbulence near the free surface is partly dissipated and partly diffused and convected downwards. As the waterfront moves toward the beach, turbulent energy is dampened and becomes evenly distributed along the vertical.

Just before backwash, most of the turbulence energy has been damped and the overall turbulence level lowers to a minimum. During the backwash phase, with a gravity-dominated flow, turbulence energy starts to increase again, especially near the bottom. This appears to be the only source of turbulence, except for some possible occasional moving hydraulic jumps. In fact, in the most landward section (Fig. 6c) energy appears to increase rapidly at 0.5δ as a consequence of a bore generation; then it is damped and convected in the mean flow direction (Fig. 6b). Finally (Fig. 6a) it increases again due to the diffusion of wall turbulence.

The mean value of turbulence energy is almost constant when moving landward from sec. 7 to sec. 8; the maximum value was not detected, due to the LDV unlocking in the presence of the roller. The apparent equal levels of maximum turbulent energy, around 200 cm^2/s^2, are probably due to a fixed S/N ratio that unlocks the LDV signal.

Similar behaviour was noted for experiments with 2.5-s (also shown in Figs. 4~6) and 2.0-s wave periods (not reported), even though the breaking type is different for the 2 shorter periods.

Fig. 7 shows some normalised energy spectral densities of the horizontal velocity fluctuations, evaluated for the 3.0-s wave in sec. 8. They are phase-averaged. The maximum expected frequency could be evaluated assuming that $\Lambda\, k_{max} \geq 100$, where k_{max} is the wave number of micro vortices (Nezu and Nakagawa, 1993). Assuming a macro scale scaled with the flow thickness, the maximum frequency expected in the viscous range is $f_{max} \approx (50/\pi)(\tilde{u}_0/\delta) = 250$ Hz (the amplitude $\tilde{u}_0 \sim 0.5$ m/s and $\delta \sim 3$ cm used as velocity scale). The acquisition frequency is much lower

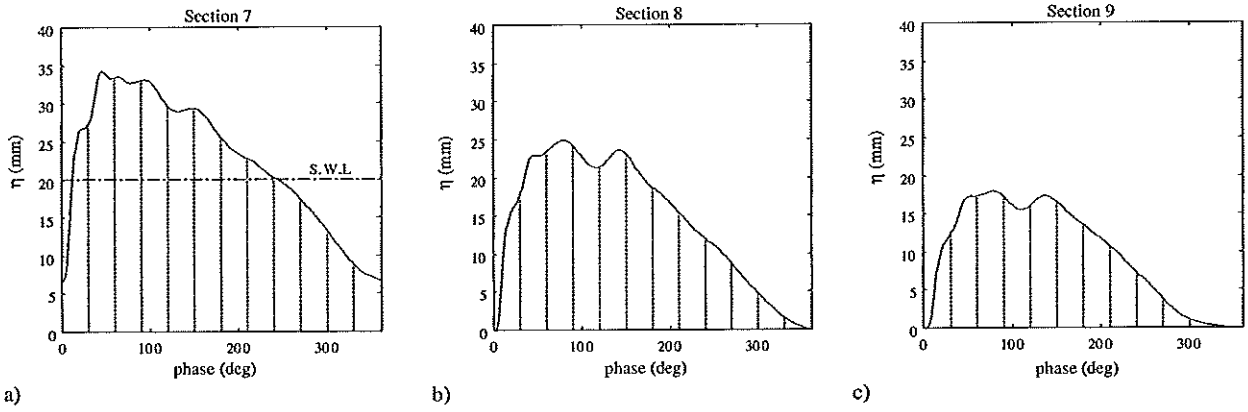

Fig. 3 Phase-averaged free surface, for wave with period T = 3.0 s, in sec. 7a, 8b and 9c. Phase is triggered to minimum water level in sec. 8 for all sections.

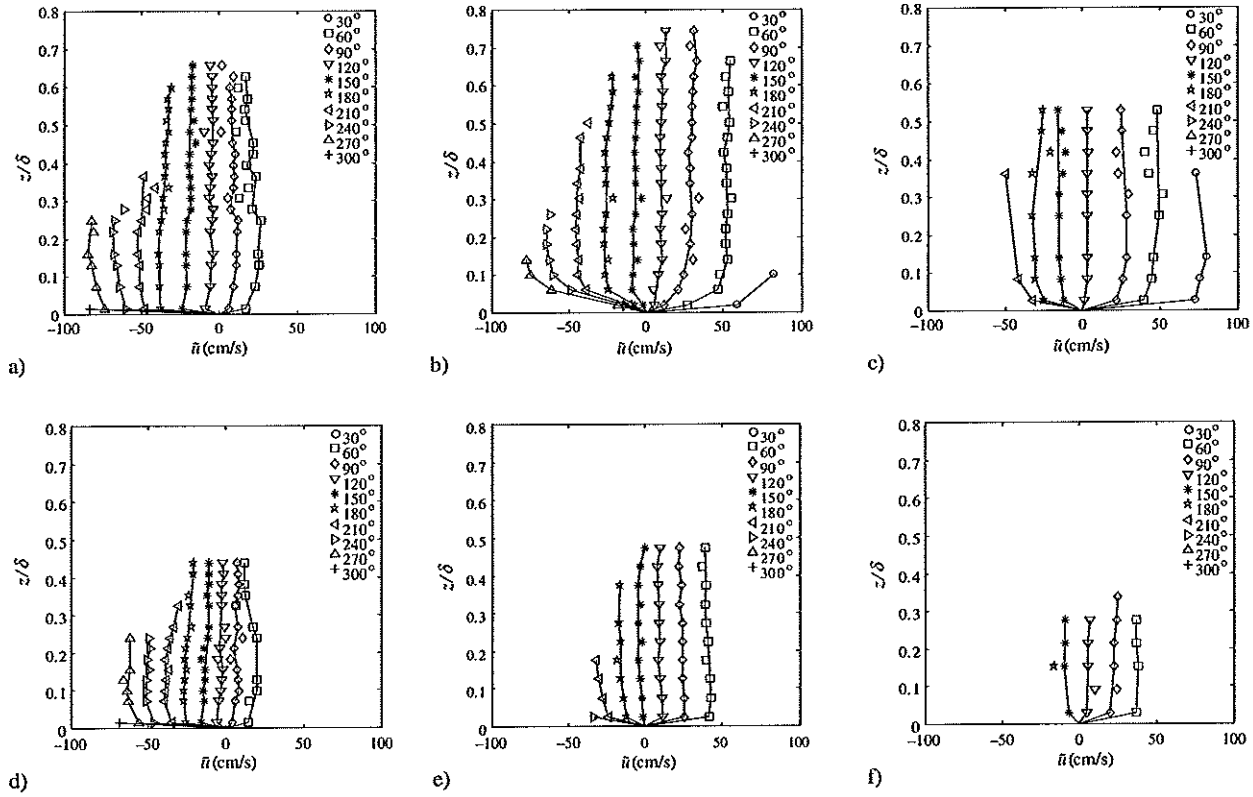

Fig. 4 Phase-averaged horizontal velocities as function of nondimensional depth. Wave with period T = 3.0 s, sec. 7a, 8b and 9c; wave with period T = 2.5 s, sec. 7d, 8e and 9f. Phase is triggered to minimum water level in sec. 8 for all 3 sections.

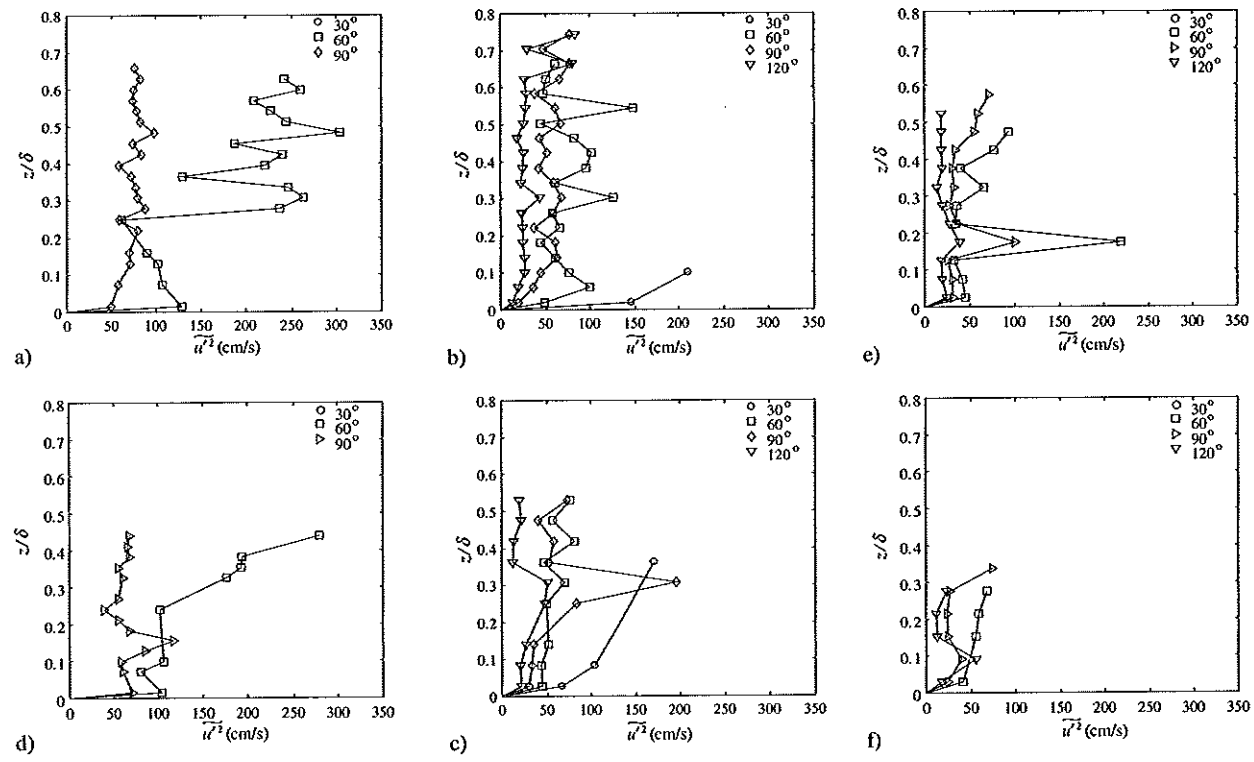

Fig. 5 Phase-averaged horizontal turbulent energy during up-rush phase as function of nondimensional depth. Wave with period T = 3.0 s, sec.7a, 8b and 9c; wave with period T = 2.5 s, sec.7d, 8e and 9f. For phase triggering, see caption in Fig. 4.

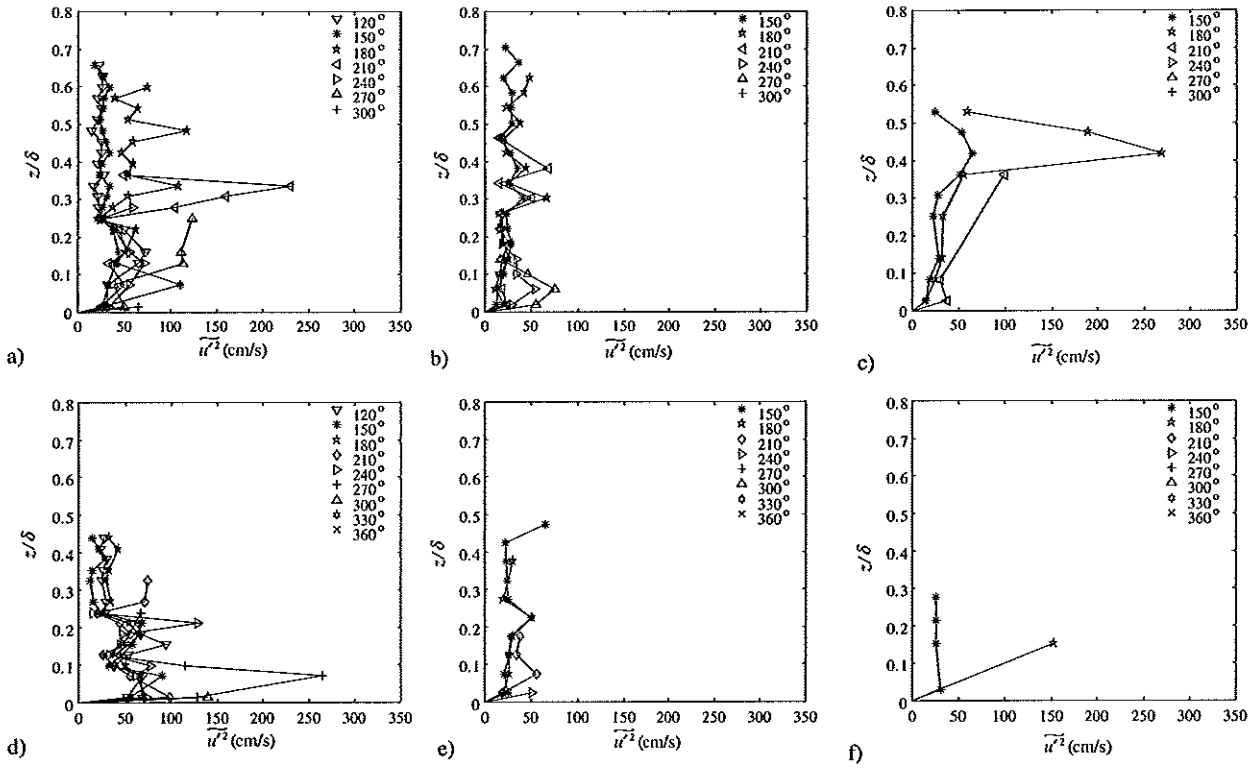

Fig. 6 Phase-averaged horizontal turbulent energy during backwash phase as function of nondimensional depth. Wave with period T = 3.0 s, sec. 7a, 8b and 9c; wave with period T = 2.5 s, sec. 7d, 8e and 9f. For phase triggering, see caption in Fig. 4.

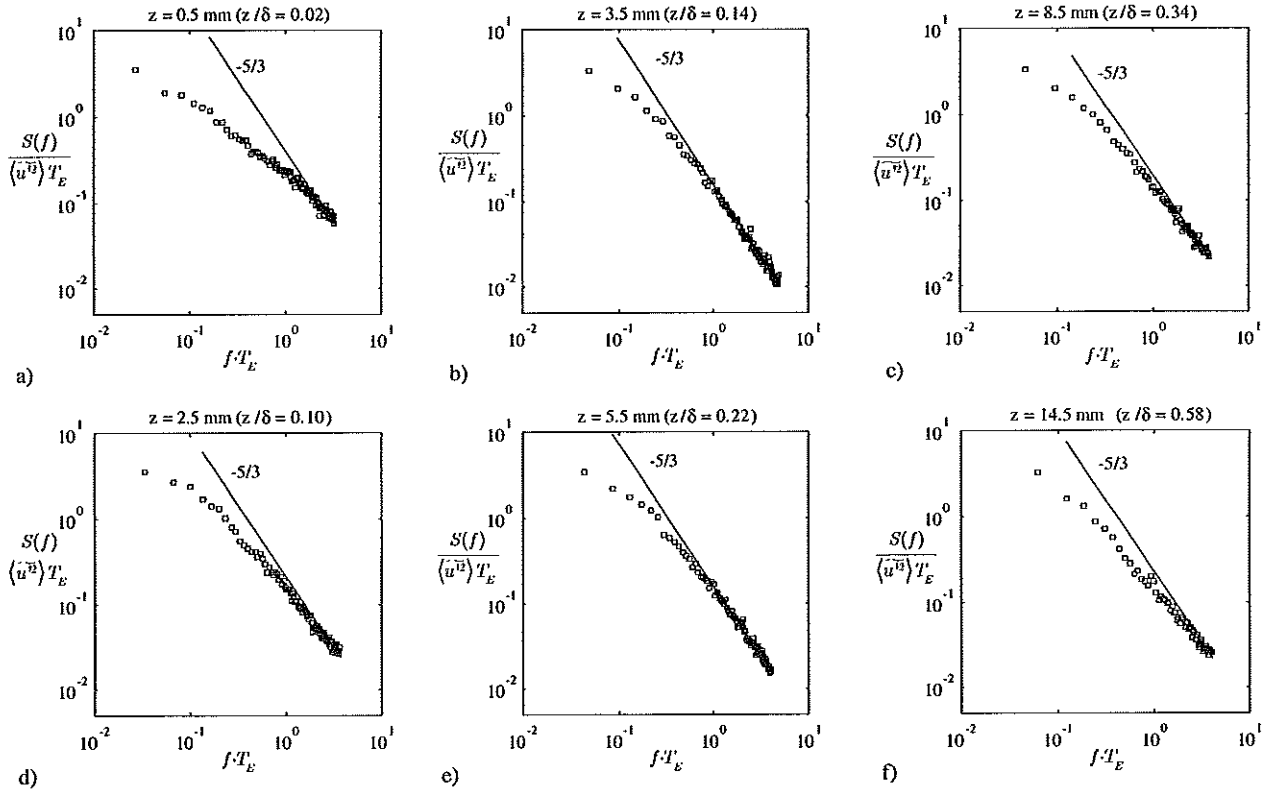

Fig. 7 Examples of phase-averaged energy spectral density of horizontal velocities, for wave with period T = 3.0 s, in sec. 8

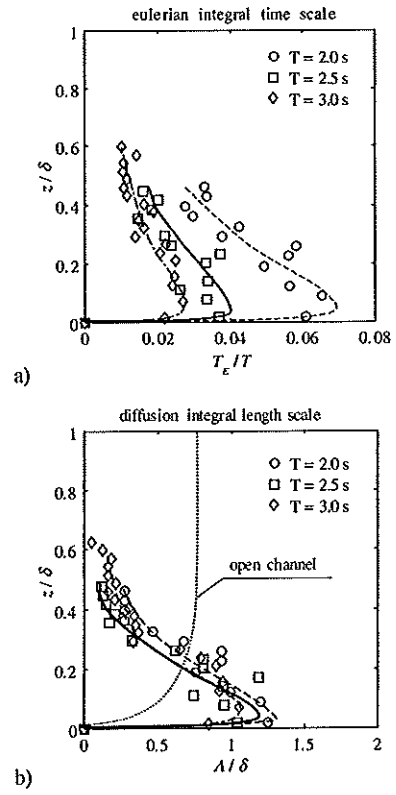

Fig. 8 Eulerian integral time scale and diffusion integral length scale for all waves as a function of nondimensional depth in sec. 7

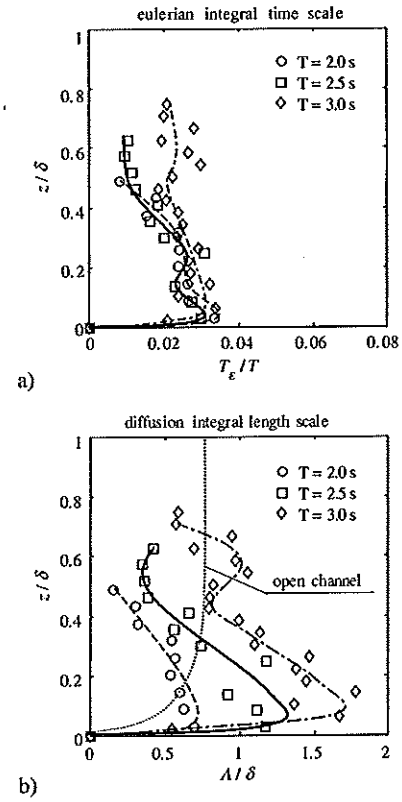

Fig. 9 Eulerian integral time scale and diffusion integral length scale for all waves as a function of nondimensional depth in sec. 8

and the Nyquist frequency is limited to 50 Hz. As a consequence, the spectra obtained are not detailed enough to cover the dissipative turbulence ranges. The problem is less evident in the field, where the flow thickness is much higher and the maximum frequency is much more limited. The slope of velocity spectra at high frequencies (higher than 5 Hz) is approximated by a –5/3 slope, corresponding to an equilibrium range, at least for the levels $0.14 \le z/\delta \le 0.22$. Similar behaviour was seen for the 2 other wave periods in sec. 7. In all the other tests (T = 2.0 and 2.5 s in sec. 8 and 9) the spectra show a slope of less than –5/3: This is because the range of equilibrium can only be achieved for $Re_i > 10^5$, with $Re_i = (u\Lambda)/\nu$ and u and Λ being the velocity and the integral scales of turbulence (the latter is often defined as the diffusion length scale). In all present experiments Re_i is of the order of 10^3 and the equilibrium range is not reached (as happens in most laboratory conditions).

Figs. 8~10 show the Eulerian time integral scale T_E and the corresponding diffusion length scale Λ. The time integral scale, an indicator of turbulence persistence, increases from the bottom up to the vertical elevation of $z/\delta \approx 0.08$ and then decreases more or less monotonously towards the free surface. An exception was the 2.0-s wave in sec. 9, where there is a constant increase.

A similar trend is evident in the diffusion length scales (Figs. 8b~10b). Direct comparison with other literature on results is not simple because most of the existing studies refer to the surf zone; moreover the results are often presented in nondimensional form with respect to the still water depth that is very low or completely lacking in the swash zone. However, the behaviour of the length scales obtained in the present experiments is very similar to that obtained in the inner surf zone by Pedersen et al. (1998). They obtained the integral spatial scale directly from spatial correlation measurements and found substantially Λ increasing from the bottom up to a value $\Lambda/D \approx 0.3$ (D is the still water depth) reached at the dimensionless distance $z/D \approx 0.15$ and then slowly decreasing (at quite constant values) towards the free surface.

In all the sections it is quite evident that diffusion integral length scales are the same as δ and comply with results obtained by Flick and George (1990). Length scale profiles show a substantial coincidence of the 3 different wave periods only in sec. 7; in the other 2 sections (8 and 9) the profiles are clearly separated. This indicates a similar vortex structure immediately after breaking and a different vortex evolution on the beach depending on the wave period; for longer waves, the fluid flow tends to preserve the vortex structure, while for shorter waves the macro vortex is destroyed quite rapidly. This can be described as a sort of turbulence tuning to the main flow frequency. In sec. 7 the maximum value is $\Lambda/D \approx 1.2$; in sections 8 and 9 the maximum value of Λ/D is between 0.7 and 1.8. Generally speaking, longer period waves induce bigger integral length scales. The shorter wave in the upper section has both time and length integral scales increasing up to the free surface and is more similar to those found in an open channel, i.e. in a bottom-controlled turbulence flow field. That can be the result of rapid dampening of the roller-generated turbulence and a rapid adaptation to local conditions.

The measured length scales are higher than those found in an open channel (dotted lines); they also have a maximum near the bottom, while in an open channel the maximum is around $0.6h$ where h is the water depth (Nezu and Nakagawa, 1993).

The eddy viscosity drafted in Fig. 11 is also much higher than

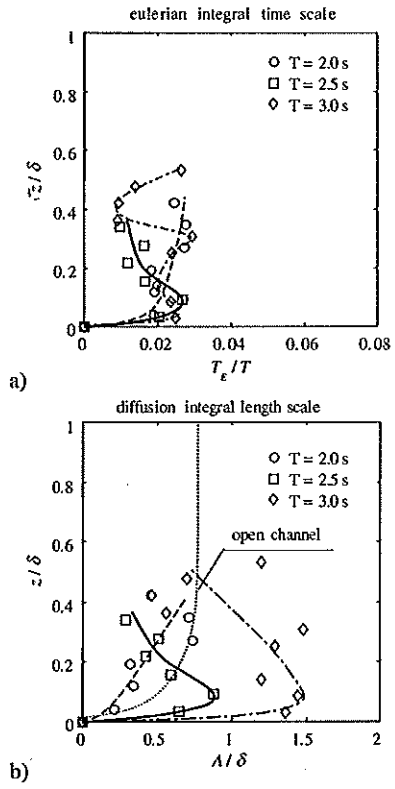

Fig. 10 Eulerian integral time scale and diffusion integral length scale for all waves as a function of nondimensional depth in sec. 9

that obtained in a uniform stream of equivalent depth and friction velocity. The latter is usually assumed to be parabolic:

$$\nu_t = k u_* z\left(1-\frac{z}{\delta}\right) \tag{13}$$

where u_* is the friction velocity and k the von Kármán constant. The friction velocity computed using the first level measurements (z = 0.5 mm) is of, say, 5 cm/s; the eddy viscosity in an equivalent uniform stream in an open-channel flow has a maximum in the middle equal to ~1.3×10^{-4} m^2/s. The mixing level is higher and the consequence is an almost uniform velocity profile; momentum exchange is very efficient and possible deviations from uniform velocity are smoothed over very quickly. It is important to remember that from a phenomenological point of view, eddy viscosity is the product of vertical fluctuating velocity (or an estimator) and the vertical length scale; the assumption of equal vertical and horizontal length scales is certainly not true near the bottom and the free surface, where vortices are stretched and interact with the boundaries.

CONCLUSIONS

Some features of the flow field and the turbulence induced by a broken wave in the swash zone have been presented.

- Fluid velocity is almost uniform along the vertical in the sections after breaking, especially during the up-rush.
- Turbulence is roller-controlled during the up-rush, with higher energy near the surface; it is controlled from the bottom during backwash.
- Turbulence spectra show a smaller slope than the classical Kolgomorov slope for the equilibrium range: near the bottom and near the surface, where the anisotropy is strong, the slope is equal to ~ −1 and ~ −4/3. A possible explanation is a small Reynolds number, $Re_l = (u\Lambda)/\nu << 10^5$.
- The integral length scales reach a maximum near the bottom, where the macro vortices are strongly stretched. Their behaviour near the free surface could not be detected because the air bubbles unlocked the LDV; it is expected that there is a second maximum also at this point. The measured length scale is several times the length scale of an equivalent open channel; the difference can easily be the result of the roller generated by the breaker that strongly dominates the flow field.
- The eddy diffusivity, computed simply as the integral horizontal space scale time the turbulence velocity scale (based on the horizontal velocity), is a higher order of magnitude than in an equivalent open channel flow; the comparison can be useful even though conceptually the vertical eddy viscosity is connected to the vertical length scale and the turbulence velocity scale based on turbulent energy. The friction velocity is very high due to the breaker turbulence penetration into the wall boundary layer (not shown in this paper); the mixing level is generally high and justifies the almost uniform velocity profile.

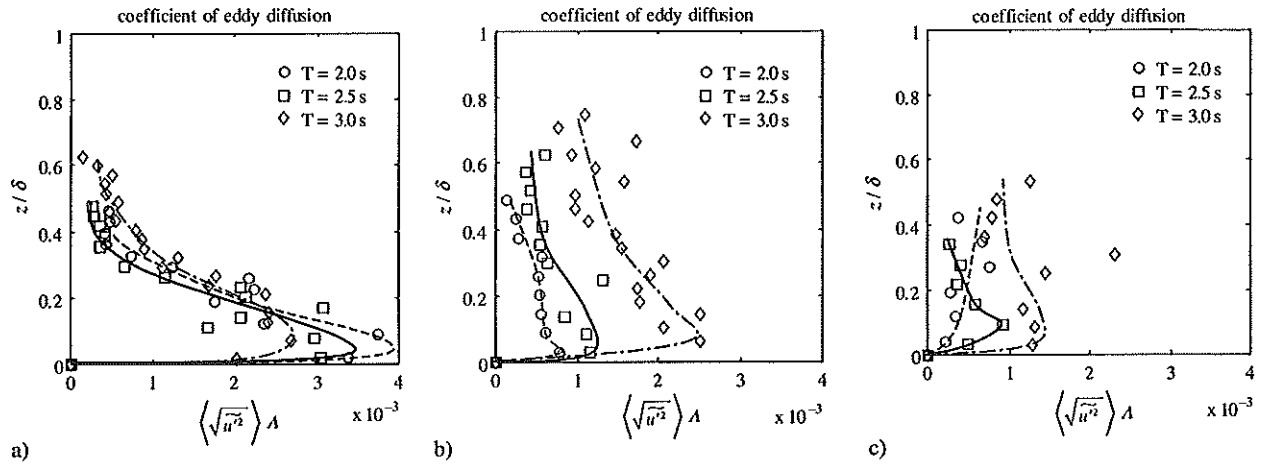

Fig. 11 Coefficient of eddy diffusion as a function of nondimensional depth in sections 7a, 8b and 9c

ACKNOWLEDGEMENTS

This work is undertaken as part of the MAST III - SASME Project (Surf and Swash Zone Mechanics) supported by the Commission of the European Communities, Directorate General Research and Development, under Contract No. MAS3-CT97-0081. We wish to express our thanks to Stefano Sadun, Matteo Tirindelli and the technicians Mauro Gioli and Muzio Mascherini for their valuable collaboration in carrying out the experiments.

REFERENCES

Abbott, MB, Petersen, HM, and Skovgaard, O (1978). "On the Numerical Modelling of Short Waves in Shallow Water," *J Hydr Res*, Vol 16, No 3, pp 173-203.

Abbott, MB (1979). *Computational Hydraulics, Elements of the Theory of Free Surface Flows*, Pintam Adv Publ Program, Pintam Publ, London.

Deigaard, R, and Fredsøe, J (1989). "Shear Stress Distribution in Dissipative Water Waves," *Coastal Eng*, Vol 13, pp 357-378.

Drago, M, and Iovenitti, L (1995). "The Modelling of Plunging Breakers by the Introduction of a *K-l* Turbulence Closure Model," *Proc Coastal Dyn*, ASCE, pp 317-328.

Flick, RE, and George, RA (1990). "Turbulence Scales in the Surf and Swash," *Proc 22nd Conf Coastal Eng*, ASCE, pp 547-566.

Gourlay, MR (1992). "Wave Set-up, Wave Run-up and Beach Water Table: Interaction Between Surf Zone Hydraulics and Groundwater Hydraulics," *Coastal Eng*, Vol 17, pp 93-144.

Karambas, T, and Koutitas, C (1992). "A Breaking Wave Propagation Model Based on the Boussinesq Equations," *Coastal Eng*, Vol 18, pp 1-19.

Lin, P, and Liu, LF (1998). "Breaking Waves in the Surf zone," *J Fluid Mech*, Vol 359, pp 239-264.

Mei, CC (1989). "The Applied Dynamics of Ocean Surface Waves," *Advanced Series on Ocean Eng*, Vol 1, World Sci Publ.

Nadaoka, K, Hino, M, and Koyano, Y (1989). "Structure of the Turbulent Flow Field Under Breaking Waves in the Surf Zone," *J Fluid Mech*, Vol 204, pp 359-387.

Nezu, I and Nakagawa, HI, (1993). *Turbulence in Open Channel Flows*. IAHR Monograph Series.

Pedersen, C, Deigaard, R, and Sutherland, J (1998). "Measurements of the Vertical Correlation in Turbulence Under Broken Waves," *Coastal Eng*, Vol 35, pp 231-249.

Petti, M (1988). "Second Order Analysis of Shallow-Water Spectra," *Il Nuovo Cimento*, Vol 11 C, N 5-6.

Petti, M (2001). "Influence of the Seiche on Turbulence Estimates." *In preparation.*

Reynolds, AJ (1974). *Turbulent Flows in Engineering*, Wiley Interscience Publ, London.

Rodriguez, A, Sanchez-Arcilla A, Redondo, JM, and Mos, C (1999). "Macroturbulence Measurements with Electromagnetic and Ultrasonic Sensors: A Comparison Under High-turbulent Flows," *Experiments in Fluid*, Vol 27, pp 31-42.

Schäffer, HA, Madsen, PA, and Deigaard R (1993). "A Boussinesq Model for Waves Breaking in Shallow Water," *Coastal Eng*, Vol 20, pp 185-202.

Stive, MJF (1980). "Velocity and Pressure Field of Spilling Breaker," *Proc 17th Conf Coastal Eng*, ASCE, pp 547-566.

Svendsen, IA (1984). "Wave Heights and Set-up in a Surf Zone," *Coastal Eng*, Vol 8, pp 303-329.

Ting, FCK, and Kirby, JT (1994). "Observation of Undertow and Turbulence in a Laboratory Surf Zone," *Coastal Eng*, Vol 24, pp 51-80.

Ting, FCK, and Kirby, JT (1995). "Dynamics of Surf-zone Turbulence in a Strong Plunging Breaker," *Coastal Eng*, Vol 24, pp 177-204.

Ting, FCK, and Kirby, JT (1996). "Dynamics of Surf-zone Turbulence in a Spilling Breaker," *Coastal Eng*, Vol 27, pp 131-160.